Constraints on Mimas' interior from Cassini ISS libration measurements

R. Tajeddine *et al.*

Science **346**, 322 (2014);
DOI: 10.1126/science.1255299

to the changes observed by MRI. Future experiments can assess whether new myelinating cells are required for other types of learning as well.

REFERENCES AND NOTES

1. W. D. Richardson, K. M. Young, R. B. Tripathi, I. McKenzie, *Neuron* **70**, 661–673 (2011).
2. L. E. Rivers *et al.*, *Nat. Neurosci.* **11**, 1392–1401 (2008).
3. K. M. Young *et al.*, *Neuron* **77**, 873–885 (2013).
4. S. L. Bengtsson *et al.*, *Nat. Neurosci.* **8**, 1148–1150 (2005).
5. J. Scholz, M. C. Klein, T. E. Behrens, H. Johansen-Berg, *Nat. Neurosci.* **12**, 1370–1371 (2009).
6. Y. Hu *et al.*, *Hum. Brain Mapp.* **32**, 10–21 (2011).
7. C. Sampaio-Baptista *et al.*, *J. Neurosci.* **33**, 19499–19503 (2013).
8. B. Emery *et al.*, *Cell* **138**, 172–185 (2009).
9. M. Koenning *et al.*, *J. Neurosci.* **32**, 12528–12542 (2012).
10. H. Bujalka *et al.*, *PLOS Biol.* **11**, e1001625 (2013).
11. S. Srinivas *et al.*, *BMC Dev. Biol.* **1**, 4 (2001).
12. S. Hippenmeyer *et al.*, *PLOS Biol.* **3**, e159 (2005).
13. D. Liebetanz *et al.*, *Exp. Neurol.* **205**, 207–213 (2007).
14. N. Hibbits, R. Pannu, T. J. Wu, R. C. Armstrong, *ASN Neuro* **1**, 153–164 (2009).
15. M. Hildebrand, *Bioscience* **39**, 766–775 (1989).
16. S. Grillner, *Neuron* **52**, 751–766 (2006).
17. P. M. Schalomon, D. Wahlsten, *Brain Res. Bull.* **57**, 27–33 (2002).
18. B. Milner, L. R. Squire, E. R. Kandel, *Neuron* **20**, 445–468 (1998).
19. R. R. Sturrock, *Neuropathol. Appl. Neurobiol.* **6**, 415–420 (1980).
20. G. S. Tomassy *et al.*, *Science* **344**, 319–324 (2014).
21. Y. Bakiri *et al.*, *Neuroscience* **158**, 266–274 (2009).
22. D. E. Bergles, R. Jabs, C. Steinhäuser, *Brain Res. Rev.* **63**, 130–137 (2010).
23. V. Gallo, J. M. Mangin, M. Kukley, D. Dietrich, *J. Physiol.* **586**, 3767–3781 (2008).
24. P. P. Maldonado, M. Vélez-Fort, M. C. Angulo, *J. Anat.* **219**, 8–17 (2011).
25. R. D. Fields, *Semin. Cell Dev. Biol.* **22**, 214–219 (2011).
26. C. Simon, M. Götz, L. Dimou, *Glia* **59**, 869–881 (2011).
27. E. M. Gibson *et al.*, *Science* **344**, 1252304 (2014).
28. B. A. Barres, M. C. Raff, *Nature* **361**, 258–260 (1993).
29. Q. Li, M. Brus-Ramer, J. H. Martin, J. W. McDonald, *Neurosci. Lett.* **479**, 128–133 (2010).
30. M. Makinodan, K. M. Rosen, S. Ito, G. Corfas, *Science* **337**, 1357–1360 (2012).
31. J. M. Mangin, P. Li, J. Scafidi, V. Gallo, *Nat. Neurosci.* **15**, 1192–1194 (2012).
32. H. Wake, P. R. Lee, R. D. Fields, *Science* **333**, 1647–1651 (2011).
33. H. Takeuchi *et al.*, *J. Neurosci.* **30**, 3297–3303 (2010).
34. A. A. Schlegel, J. J. Rudelson, P. U. Tse, *J. Cogn. Neurosci.* **24**, 1664–1670 (2012).

ACKNOWLEDGMENTS

We thank the staff of the Center for Electron Microscopy and Bio-Imaging Research, Iwate Medical University, and U. Dennehy and M. Grist (University College London) for technical help and our colleagues in the Wolfson Institute for Biomedical Research for encouragement and suggestions. W.D.R. thanks T. Richardson for stimulating discussions. The study was supported by the European Research Council (grant agreement 293544), the UK Medical Research Council, the Wellcome Trust, and Grants-in-Aid from the Japanese Ministry of Education, Culture, Sports, Science and Technology. W.D.R. and K.T. acknowledge an Invitation Fellowship from the Japan Society for Promotion of Science. I.M. was supported by a Royal Society USA/Canada Exchange Fellowship, J.P.d.F. by a fellowship from the Portuguese Fundação para a Ciência e a Tecnologia, and B.E. by a Career Development Fellowship from the Australian National Health and Medical Research Council. *Pdgfra-CreER^{T2}* and *Sox10-CreER^{T2}* mice can be obtained by request through www.e-lucid.com/ with a material transfer agreement. *Myrf(flox)* mice can be obtained from Jackson Laboratories, strain 010607. The supplementary materials include additional data.

SUPPLEMENTARY MATERIALS

www.sciencemag.org/content/346/6207/318/suppl/DC1
Materials and Methods
Supplementary Text
Figs. S1 to S7
References (*35*, *36*)
Movies S1 to S5

17 April 2014; accepted 14 August 2014
10.1126/science.1254960

REPORTS

PLANETARY GEOLOGY

Constraints on Mimas' interior from Cassini ISS libration measurements

R. Tajeddine,[1,2,3]* N. Rambaux,[2,3] V. Lainey,[2] S. Charnoz,[4] A. Richard,[2] A. Rivoldini,[5] B. Noyelles[6]

Like our Moon, the majority of the solar system's satellites are locked in a 1:1 spin-orbit resonance; on average, these satellites show the same face toward the planet at a constant rotation rate equal to the satellite's orbital rate. In addition to the uniform rotational motion, physical librations (oscillations about an equilibrium) also occur. The librations may contain signatures of the satellite's internal properties. Using stereophotogrammetry on Cassini Image Science Subsystem (ISS) images, we measured longitudinal physical forced librations of Saturn's moon Mimas. Our measurements confirm all the libration amplitudes calculated from the orbital dynamics, with one exception. This amplitude depends mainly on Mimas' internal structure and has an observed value of twice the predicted one, assuming hydrostatic equilibrium. After considering various possible interior models of Mimas, we argue that the satellite has either a large nonhydrostatic interior, or a hydrostatic one with an internal ocean beneath a thick icy shell.

Among Saturn's inner main moons, Mimas is the smallest (radius ~198 km) and closest to the planet (semimajor axis ~189,000 km). Along with Enceladus, Tethys, Dione, and Rhea, it is classified as a mid-sized icy moon; the origin of these moons is still being debated. The classical model describes their formation by accretion in the protoplanetary subnebula (*1*–*6*) or by collision between two large satellites and reaccretion of the impact ejecta (*7*, *8*), but does not explain the satellites' masses, sizes, and radial locations. A new model reconciles these parameters by forming the satellites in the rings (*9*–*11*). However, this model assumes that the primordial rings were massive and contained silicate; furthermore, Saturn must have been tidally very dissipative (*12*) to move all the mid-sized moons to their current locations.

We measured Mimas' forced librations using Cassini's ISS Narrow Angle Camera (NAC) images, using methods previously applied to Phobos (*13*, *14*), to gain insights into Mimas' interior. The measurements of rotational parameters have been proven to be a powerful tool to investigate the interior state of celestial bodies (*15*). The absence of evident geological activity on Mimas' surface (*16*) suggests that it may have a cold interior that may have helped in conserving a "fossil" record of structures within its interior. This encouraged us to investigate Mimas' rotational variations, which are directly linked to its internal structure and may inform us about its origin.

First, we developed a control point network across Mimas' surface by applying the method of stereophotogrammetry, where (*X*, *Y*, *Z*) coordinates of a surface point in the satellite's frame are projected in an image as sample (*x*) and line (*y*) coordinates in pixels. For the 3D reconstruction, each point has been observed at least twice and from two different viewing angles (*17*). After selecting recognizable landmarks from Mimas' map (*18*), a least-squares method was applied comparing the (*X*, *Y*, *Z*) coordinates of each projected point in the image to the observed ones. From this, a topographic map of 260 surface points was built (Fig. 1A), based on 2135 point measurements from 40 Cassini images with resolutions ranging from 360 to 1450 m per pixel (see table S2 for a full list of images). The mean uncertainties on a point's coordinates are estimated as ±599 m, ±731 m, and ±395 m on *X*, *Y*, and *Z* coordinates, respectively. To test our method, we rebuilt and confirmed the satellite's triaxial shape using these points (*17*, *19*).

In the photogrammetric reconstruction method described above, a rotational model of Mimas is used (*17*). The better this model describes Mimas' rotation, the smaller the χ^2 errors from the topographic reconstruction. Hence, we repeatedly built Mimas' control point network by varying its forced libration amplitudes and phases until the total value of χ^2 was minimized. The measurements (Table 1) (*17*) confirm all the theoretical values (*20*) except for the amplitude corresponding to the 0.945-day period, which is almost twice the predicted one (Fig. 1B). The uncertainty on this libration amplitude has been

[1]Department of Astronomy, Cornell University, Ithaca, NY 14853, USA. [2]IMCCE–Observatoire de Paris, UMR 8028 du CNRS, UPMC, Université Lille 1, 77 Av. Denfert-Rochereau, 75014 Paris, France. [3]Université Pierre et Marie Curie, UPMC – Paris VI, 4 Place Jussieu, 75005 Paris, France. [4]Laboratoire AIM, UMR 7158, Université Paris Diderot/CEA IRFU/CNRS, Centre de l'Orme les Merisiers, 91191 Gif-sur-Yvette Cedex, France. [5]Royal Observatory of Belgium, Avenue Circulaire 3, B-1180 Brussels, Belgium. [6]Department of Mathematics and Namur Center for Complex Systems, Université de Namur, 5000 Namur, Belgium.
***Corresponding author. E-mail: tajeddine@astro.cornell.edu**

estimated by adding Gaussian noise (taking into account all the sources of error) to the control points, and by repeatedly measuring the libration amplitude (Fig. 1C) (*17*). The final value of the libration amplitude (Table 1) is the result of a Gaussian fit to the histogram. Here, all the sources of error were considered random; by accounting for systematic errors, the highest value of uncertainty on the libration amplitude for the 0.945-day signal is ~1.5 arc min (*17*).

The mathematical expression for the physical forced libration is

$$\gamma = \sum_i \frac{H_i}{1-(\omega_i/\omega_0)^2}\cos(\omega_i t + \varphi_i) \qquad (1)$$

where ω_i and φ_i are the ith libration frequency and phase, respectively (*17*, *21*). H_i depends on the satellite's orbital dynamics and ω_0 is the system's free libration frequency, which for a solid body can be written, to the first order in eccentricity, as

$$\omega_0 = n\sqrt{3\left(\frac{B-A}{C}\right)} \qquad (2)$$

where A, B, and C are the satellite's principal moments of inertia and n is the satellite's mean motion. When the ratio $(\omega_i/\omega_0)^2$ is non-negligible in front of 1, the libration amplitude is dominated by the satellite's internal structure (*21*). Otherwise, the libration amplitude depends mainly on its orbital dynamics. The periods in Table 1 are the outcome of Mimas' orbital dynamics, creating effects of the longitudinal librations through Saturn's external gravitational torque. The strongest libration periods of ~70 and ~23 years are created by the Mimas-Tethys mean motion resonance. The period of 0.945 days is the anomalistic orbital period (perigee to perigee), which is slightly longer than the orbital period of 0.942 days; it is due to the precession of the pericenter, and the last three periods are directly linked to the precession of Mimas' pericenter. Using a triaxiality of $(B - A)/C$ = 0.06 (*22*), the only amplitude that depends on the interior is the one with a period of 0.945 days (Table 1), which has been computed (*20*) assuming that Mimas is in hydrostatic equilibrium. The measured libration amplitude of 50.3 ± 1 arc min corresponds to a solid Mimas of triaxiality $(B-A)/C = 0.091 \pm 0.001$, which is surprisingly high.

To better understand such a large measured libration amplitude, we investigated five possible interior models of Mimas (*17*) to assess whether they could reproduce the observed libration: a homogeneous distribution of mass, a two-layer body in hydrostatic equilibrium, a mass anomaly under crater Herschel, a nonhydrostatic core, and an internal ocean. The results show that the cases of a homogeneous and a two-layer equilibrium body (*17*) can be discarded because the libration amplitude for these models is much smaller that our measured value (between 25.5 and 29 arc min).

Herschel, the largest crater on Mimas, is located at a longitude of 111.76°W, near Mimas' equator, and is 140 km wide and 10 km deep. The missing material from the impact basin modifies the satellite's moments of inertia. Moreover, as a consequence of the impact, a large subsurface mass anomaly could have formed below the crater. As in analyses of the effect of the Stickney crater on the libration of Phobos (*23*, *24*), we computed Mimas' libration amplitude by considering the presence of a large volume with porosity up to 45% (*25*) at depths as much as 70 km under Herschel (*17*). The effect of the basin increases the libration amplitude by ~1 arc min, which is not enough to explain the observed libration amplitude. On the other hand, the macroporosity increases the libration amplitude up to 46 arc min, for which the mass anomaly is so big that (if currently present) it would cause a reorientation of Mimas about the polar axis by 8°. Such reorientation is inconsistent with the present-day location of Herschel.

We also tested a model of Mimas with a nonhydrostatic shaped core. Any change in the core's shape must maintain the configuration of the satellite's principal moments of inertia where $A \leq B \leq C$. This can only be done by increasing the core's axis a_c, yielding a decrease in the b_c and/or c_c axes in order to conserve the core's total mass. In this model, we varied the densities of the shell and the core between 700 kg/m^3 and 950 kg/m^3 and between 1200 kg/m^3 and 3300 kg/m^3, respectively. Our calculations show that in order to explain the observed libration, the core should be elongated (compared to an equivalent model in hydrostatic equilibrium), between 20 and 60 km, on each side of the core's longest axis, increasing proportionally with the shell and core densities (*17*). Our calculations show that the suggested excess in topography for a silicate body such as Mimas' suggested core is supportable (*17*). Although this interior model seems simplistic (as an unlimited number of models with core deformations could be developed), it quantifies the

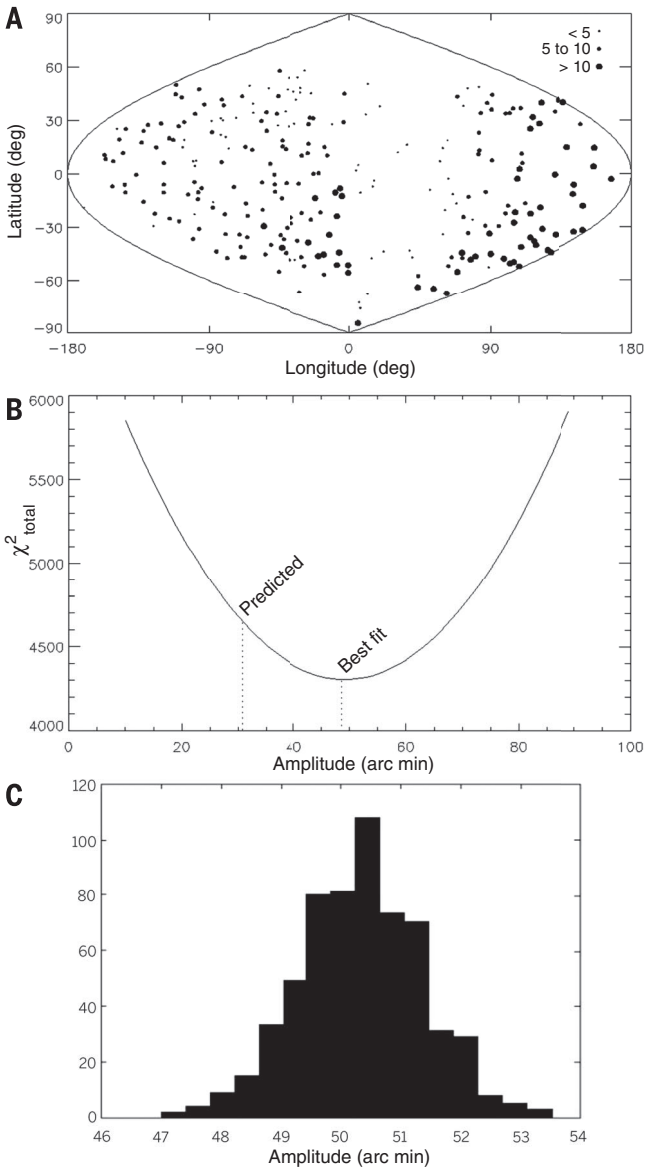

Fig. 1. Mimas' control point network and libration measurement. (**A**) A map of the used control point network of Mimas, where size represents the number of times a point has been observed. The map has poor coverage at low longitudes but good coverage around the Herschel crater (longitude 111.76°W, latitude –1.38°). Mimas' north pole has been observed only once, preventing access to any topographic information about this area. (**B**) A plot of the non-normalized total χ^2 (obtained from the map reconstruction) as a function of the libration amplitude of the period, 0.945 days. The number of degrees of freedom is 4269, as each point measurement provides one data point in sample and one in line. However, this plot is the result of only one fit. (**C**) Histogram of 600 solutions for the libration amplitude, when adding 1σ (of the estimated uncertainties on points) of Gaussian noise to the control points' positions. The Gaussian fit to the histogram gives the final solution for the libration amplitude (with its estimated uncertainty) as shown in Table 1.

required excess in the core's topography in order to explain the high libration amplitude. One question is whether such core should have effects on the satellite's global shape. Assuming that the shell is fully relaxed (which may not be necessarily the case), the effect of the core's shape on the global geoid (*17*) is not consistent with the satellite's observed shape (*19*). The mean offsets to the observations are about 2 km, –1.5 km, and –1.4 km in *a*, *b*, and *c* axes, respectively. Hence, the satellite should be more elongated. In fact, any anomaly in Mimas' interior should ultimately have an effect on Mimas' global geoid. However, in the models we developed, the densities in the layers were assumed constant. A low-gravity body like Mimas could generate and maintain large porosity in both ice and silicates. Large lateral variations in density could result, which may not correlate with the surface topography. In fact, it has been argued (*26*) that small bodies like Enceladus or Mimas may retain oddly shaped cores as a result of their original accretion and collisional evolution.

For a body with an internal global ocean, the calculation of the libration amplitude depends mainly on the shell thickness. It depends to a lesser extent on the core-shell couplings and periodic tidal deformation (*27*, *28*) that decrease the satellite's libration amplitude (*17*). An ocean at 24 km below a viscoelastic shell (assuming a Maxwell rheology), or at 31 km below a rigid shell, is in agreement with the observed libration amplitude (Fig. 2). We considered two end-member cases for the viscosity of water ice. The low viscosity value of 10^{12} Pa·s induces the largest deformations and with it the strongest reduction of the libration amplitude. In contrast, for the high viscosity value of 10^{21} Pa·s, the deformations are small and the libration amplitude is close to the rigid case. Therefore, the ice layer has a thickness between 24 km and 31 km, depending on the value of the viscosity.

The ocean hypothesis sounds unlikely because, contrary to the findings on Enceladus, Mimas' heavily cratered surface has shown no evidence of liquid water, thermal heating, or geological activities. Radiogenic heating alone could not sustain such an ocean, because the heat produced by the core escapes through the satellite's icy shell and any ocean would freeze very quickly. One explanation could be found in Mimas' high eccentricity (~0.02), whose origin remains unexplained and may have been higher in the past. As a consequence, an ocean could have been formed and sustained by tidal heating.

We tested only few possible interior models in this work in an attempt to explain the observed libration amplitude, and many others could be developed. Among those that we suggested, only two are consistent with our observations: a non-hydrostatic core and a subsurface ocean. An ocean could have plausible explanations. However, the discrimination between the suggested models could be done by mapping of Mimas' gravity field that could reveal any possible mass anomalies, measuring the tidal dissipation in Mimas using Cassini's accurate astrometry (*29*), or measuring the heat flux at its surface. In any case, the measurement of the physical forced librations using Cassini ISS images shows surprising evidence that Mimas is more complex than we thought.

Table 1. Comparison of the measured forced libration's amplitudes and phases to theoretical ones (*19*). The phases corresponding to signals at 225.04, 227.02, and 223.09 days have not been measured because of their close periods and low amplitudes. The last column shows how the libration amplitude depends on the satellite's internal structure. All amplitudes here are positive, and the phase of the 0.945-day libration is out of phase by π with respect to the forcing one.

Period (days)	Theoretical amplitude (arc min)	Measured amplitude (arc min)	Theoretical phase at J2000 (deg)	Measured phase at J2000 (deg)	$(\omega_i/\omega_O)^2$
25772.62	2616.6	2631.6 ± 3.0	51.35	52.9 ± 0.9	7×10^{-9}
8590.87	43.26	44.5 ± 1.1	–25.91	–18 ± 3.2	6×10^{-8}
0.945	26.07	50.3 ± 1.0	101.35	107.7 ± 0.8	5.52
225.04	7.82	7.5 ± 0.8	–157.74	—	9×10^{-5}
227.02	3.65	2.9 ± 0.9	–119.03	—	9×10^{-5}
223.09	3.53	3.3 ± 0.8	–16.31	—	9×10^{-5}

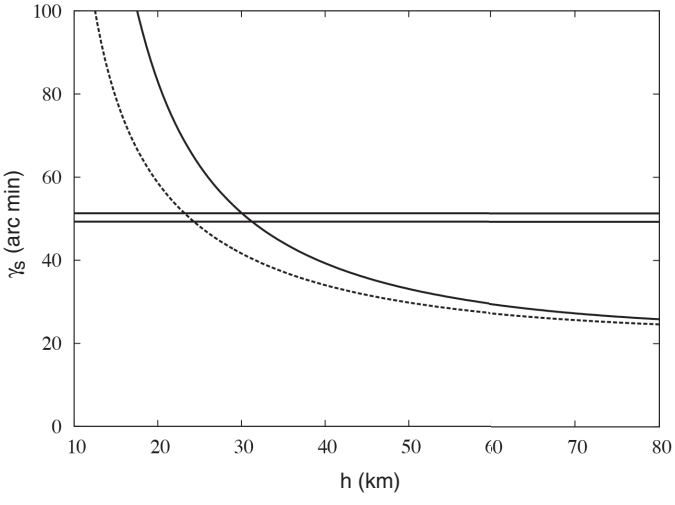

Fig. 2. Libration amplitude (γ_s) as a function of the icy shell thickness (h) for Mimas with a subsurface global ocean. The solid line represents a model with rigid solid layers, pressure, and internal gravitational coupling. The dashed line represents the same model that includes viscoelastic deformations. Horizontal lines represent 1σ range of the observed libration amplitude, 50.3 ± 1.0 arc min.

REFERENCES AND NOTES

1. R. M. Canup, W. R. Ward, *Astron. J.* **124**, 3404–3423 (2002).
2. R. M. Canup, W. R. Ward, *Nature* **441**, 834–839 (2006).
3. I. Mosqueira, P. R. Estrada, *Icarus* **163**, 198–231 (2003).
4. I. Mosqueira, P. R. Estrada, *Icarus* **163**, 232–255 (2003).
5. M. Ogihara, S. Ida, *Astrophys. J.* **753**, 60 (2012).
6. T. Sasaki, G. R. Stewart, S. Ida, *Astrophys. J.* **714**, 1052–1064 (2010).
7. Y. Sekine, H. Genda, *Planet. Space Sci.* **63–64**, 133–138 (2012).
8. E. Asphaug, A. Reufer, *Icarus* **233**, 544 (2012).
9. S. Charnoz, J. Salmon, A. Crida, *Nature* **465**, 752–754 (2010).
10. S. Charnoz *et al.*, *Icarus* **216**, 535–550 (2011).
11. A. Crida, S. Charnoz, *Science* **338**, 1196–1199 (2012).
12. V. Lainey *et al.*, *Astrophys. J.* **752**, 14 (2012).
13. T. C. Duxbury, J. D. Callahan, *Icarus* **77**, 275–286 (1989).
14. K. Willner *et al.*, *Earth Planet. Sci. Lett.* **294**, 541–546 (2010).
15. J. L. Margot, S. J. Peale, R. F. Jurgens, M. A. Slade, I. V. Holin, *Science* **316**, 710–714 (2007).
16. P. M. Schenk, *Lunar Planet. Sci. Conf.* **42**, 2729 (2011).
17. See supplementary materials on *Science* Online.
18. T. Roatsch *et al.*, *Planet. Space Sci.* **57**, 83–92 (2009).
19. P. C. Thomas, *Icarus* **208**, 395–401 (2010).
20. B. Noyelles, Ö. Karatekin, N. Rambaux, *Astron. Astrophys.* **536**, A61 (2011).
21. N. Rambaux, J. C. Castillo-Rogez, J. G. Williams, Ö. Karatekin, *Geophys. Res. Lett.* **37**, 4202 (2010).
22. S. F. Dermott, P. C. Thomas, *Icarus* **73**, 25–65 (1988).
23. N. Rambaux, J. C. Castillo-Rogez, S. Le Maistre, P. Rosenblatt, *Astron. Astrophys.* **548**, A14 (2012).
24. E. Asphaug, H. J. Melosh, *Icarus* **101**, 144–164 (1993).
25. W. B. Durham, W. B. McKinnon, L. A. Stern, *Geophys. Res. Lett.* **32**, L18202 (2005).
26. W. B. McKinnon, *J. Geophys. Res.* **118**, 1775–1788 (2013).
27. T. Van Hoolst, R. M. Baland, A. Trinh, *Icarus* **226**, 299–315 (2013).
28. A. Richard, N. Rambaux, B. Charnay, *Planet. Space Sci.* **93–94**, 22–34 (2014).
29. R. Tajeddine, N. J. Cooper, V. Lainey, S. Charnoz, C. D. Murray, *Astron. Astrophys.* **551**, A129 (2013).

ACKNOWLEDGMENTS

We thank the "ENCELADE" working group, J. A. Burns, N. J. Cooper, K. Degiorgio, M. M. Hedman, C. D. Murray, P. D. Nicholson, and T. Van Hooslt for fruitful discussions and suggestions; and the anonymous reviewers for their suggestions that improved the quality of the paper. The Cassini images that were used to obtain this paper's results are available on the Planetary Data System website, pds.nasa.gov. Supported by UPMC-EMERGENCE (contract EME0911), the Cassini mission (R.T.), the European Community's Seventh Framework Program (FP7/2007-2013) under grant agreement 263466 for the FP7-ESPaCE project (R.T., N.R., and V.L.), the UnivEarthS Labex program at Sorbonne Paris Cité (ANR-10-LABX-0023 and ANR-11-IDEX-0005-02), RS/CNRS (2011/R1 ref. IE110421) (S.C.), the European Space Agency in collaboration with the Belgian Federal Science Policy Office (A.Riv.), and an FRS-FNRS postdoctoral research fellowship (B.N.).

SUPPLEMENTARY MATERIALS

www.sciencemag.org/content/346/6207/322/suppl/DC1
Materials and Methods
Figs. S1 to S11
Tables S1 to S3
References (*30*–*47*)

28 April 2014; accepted 15 September 2014
10.1126/science.1255299